Materials Today: Proceedings 62 (2022) S176–S183

Contents lists available at ScienceDirect

Materials Today: Proceedings

journal homepage: www.elsevier.com/locate/matpr

Laser micro in situ alloying of γ-Ti46.8Al1Cr0.2Si with Manganese

Sibusisiwe Motha [a], Paul Lekoadi [b], Sadiq Abiola Raji [c,d], Basebakhe Samuel Skhosane [b], Sisa Lesley Pityana [b,c], Monnamme Tlotleng [b,e,*]

[a] Department of Chemical and Metallurgical Engineering,Univeristy of the Witwatersrand, Braamfontein, Johannesburg, 2000, South Africa
[b] National Laser Centre, Council for Scientific and Industrial Research, Meiring Naudé Road, Brummeria, Pretoria, 0184, South Africa
[c] Department of Chemical, Metallurgical and Materials Engineering, Tshwane University of Technology, Staatsartillerie Road, Pretoria West, Pretoria, South Africa
[d] Department of Metallurgical Engineering, Yaba College of Technology, P.M.B. 2011 Yaba, Lagos, Nigeria
[e] Department of Mechanical Engineering Science, University of Johannesburg, Auckland Park Campus, Johannesburg, South Africa

ARTICLE INFO

Article history:
Available online 21 May 2022

Keywords:
Additive Manufacturing
Aluminium
(α_2)-Ti_3Al
(γ)-TiAl
(α_2+ γ) – duplex microstructure
Laser In Situ Alloying
Manganese

ABSTRACT

Titanium alloys have two primary phases (α + β) that are attributed to the α-stabiliser (aluminium) and β-stabiliser (niobium). The latter stabilisers shift α-phase to higher temperature while the former stabilisers shift the β-phase to lower temperatures. To extend their scope of application, (α + β)-phase titanium alloys can be micro-alloyed with β-eutetic elements (Mn, Cr, Si, Co etc) to form intermetallic compounds which are typically referred to as titanium aluminides (Ti-Al). Several intermetallic alloys can be formed in the Ti-Al phase diagram but only (α_2)-Ti_3Al and (γ)-TiAl are stable and of relevance to structural engineering since they can be used in industries spanning across energy, aerospace and tissue-engineering. In this study, a castable γ-Ti46.8Al1Cr0.2Si pre-alloyed powder, was micro-alloyed with Mn in order to examine if it can improve its tensile properties. When 1–2 at. % Mn is added to Ti-Al alloys, it is able to increase ductility, reduce oxidation resistance and shift the (α_2 + γ)/ γ to the titanium side and decrease the Al content in the γ-phase. To effectively ascertain these effects Mn feed rates were varied from 0.2 to 1.0 rpm during the micro-alloying of γ-Ti46.8Al1Cr0.2Si through in-situ laser deposition to form γ-Ti46.8Al1Cr0.2Si-(xMn). The produced clads were characterised for chemistry and microstructure using scanning electron microscope. Results concluded that Al content decrease with an increase in Mn from 56 at. % to 49 at. %. Mn of 10.16 g/min had similar properties to the non-Mn alloyed sample. Moreover, it was shown in this work that laser processing decreased the tensile and yield strength of the alloy when compared to the as-cast in previous studies, and that 2.69 g/min and 10.16 g/min are lower and upper Mn values when ductility of the master alloy is to be improved.

1. Introduction

Additive manufacturing (AM), also commonly known as 3D printing, is unlike traditional fabrication methods such as ingot casting since complex and intricate parts can be accomplished layer-wise (or additively layer by layer) relying on a computer-aided device (CAD) file [1,2]. During part printing different feedstock(s) can be used and this depends on the type of the AM platform. Feedstock such as metallic fine powder, coarse powder and metallic wires are used distinctively or as a combination to achieve desired parts. Another distinct feature of AM machineries is the energy source. A laser beam can be used to irradiate the depositing material (be it powder or wire) during laser printing, alternatively electrons are used to melt the material. These noticeable features distinctly lead to AM machineries being grouped as laser metal deposition (LMD) or electron beam melting (EBM).

LMD techniques are further classified into powder blown and powder bed systems which literature refers to direct energy deposition (DED) and selective laser melting (SLM) or sintering (SLS), respectively. The former use coarse powder while the latter sinters fine powder that has been overlaid and scrapped to almost a micron layer. In the end, in AM, applications choose the type of powder while sophistication in the CAD file determines the type

* Corresponding author.
E-mail address: MTlotleng@csir.co.za (M. Tlotleng).

https://doi.org/10.1016/j.matpr.2022.05.077
2214-7853/

of platform to be used. In general highly complex parts, that are achieved with overhangs, and detailed finish are printed from powder bed systems while DED machines are mainly used for surface re-engineering, refurbishing and for 3D printing not so highly complex structure given their limitations in motion freedom. The limitation in machine freedom is mainly due to lack of full 5-axis trigger, and the synchronization trigger motion that supposes to enable concurrent motion between the rotating table (also known as deposition platform) and the moving deposition head. This synchronised intertwine motion allows for complex parts to be DED printed without having to build pillars or support structure as is with SLM machines.

DED systems can also be referred to as direct metal deposition (DMD), direct laser metal deposition (DLMD), laser metal deposition (LMD) and laser cladding (LC). Traditionally, these platforms are able to 3D print structures from single phase metallic powders (e.g.Ti), pre-alloyed powders (e.g. Ti64), mechanically alloyed powders (Ni-Ti), reinforcements (WC-Ti) and composite (Ti-HAp) powders, Recently, there are studies that are interested in developing alloys by means of in-situ approach [3,4]. This approach involves alloying metallic structures from corresponding elemental powders or wires as feedstock. The ideal interest in multi-powder deposition research is geared towards tailored microstructures that are fit to purpose or intended applications.

Functional grade material (FGM) structures, for example, have improved mechanical properties and can be adaptive under different loads and environments. Nitinols (Ni-Ti) variations are said to have better biomedical engineering applications when compared to traditional Ti alloys given their shape memory alloy effects [5]. This field of research (laser alloy development) is fairly new and at its' infancy however, is receiving tremendous attention given the economic benefits and freedom of manufacturing that it present. Literature studies, at research and development (R&D) or technology readiness (TRL) levels, on alloy development using DED systems are mainly concerned with reactive synthesis and the forming intermetallic, which normally lead to premature structural failure.

Great attention in this regard is directed towards how titanium and aluminium (as bulk in the binary phase alloy) and the added micron alloying metals (in the ternary or more phases) react to form titanium aluminide structures (Ti-Al) that can be used for aerospace, energy and automotive industries. The challenge with manufacturing Ti-Al components from available powders using conventional or AM methods is that they are prone to manufacturing conditions given that they are very heat sensitivity.

Ti-Al alloys are regarded as the best aeronautical structural materials due to their light-weight and extensive thermo-mechanical properties. United State Patent no ÷ 5,415,831, dated ÷ May 16, 1995 revised that: "alloys based on doped intermetallics are acquiring increasing importance in materials technology because doped intermetallic possess high strength regardless of their low density"-Google Patent Search. Gamma (γ) Ti-Al are superior, in specific strength, to nickel (Ni) base super-alloys at temperatures of about 800–900 °C, but they are ductile and sensitive to process selection and conditions. Despite these observations General Electric (GE) Ti-48Al-2Nb-2Cr or 48–2-2 alloy has been reported to have commercial use in the GEnx-family engines produced by GE Aircraft Engines [6].

To date, this is the most successfully researched, developed and commercialised alloy available, followed by the Helmholtz Association of German Research Centres (GKSS, Germany) Ti-48Al-9Nb alloy; which is commercially unavailable. Ti-48Al-9Nb is mainly used for manufacturing parts that are used in high temperature applications while 48–2-2, in addition to being a high temperature application alloy, has to some degree room temperature ductility. γ-Ti46.8Al1Cr0.2Si is the infamous GKSS alloy, and has applications in the manufacturing of valves, turbocharge rotors and piston pins, and also has compromised tensile properties [7]. In this study, this duplex phase γ-Ti46.8Al1Cr0.2Si alloy, was micro-alloyed with Mn in order to improve its' tensile properties. Mn of about 1–2 at. % is able to increase ductility in the duplex phase, reduce oxidation resistance and shift the (α_2 + γ)/ γ to the titanium side and decrease the Al content in the γ-phase. This study sort to elucidate the effects of Mn on the resulting microstructure and performance mechanical properties (YS, UTS, etc) of the cast γ-Ti46.8Al1Cr0.2Si during laser in situ alloying using LMD system.

2. Experimental procedure

A commercially pure spherical powder that was supplied by GKSS, Germany and identified as GKSS castable alloy was used as receive in this study. This alloy had particle size distribution (PSD) range of + 45–70 μm and chemical formula of Ti46.8Al1Cr0.2Si. The powder morphology is shown in Fig. 1a. Manganese that was supplied by Manganese Metal Company (Pty) Ltd. (Reg No.: 71/006609/07), South Africa is shown in Fig. 1b. This powder was fractioned to PSD + 45–112 μm before laser deposition.

The powders were cladded onto Ti64 substrates using a fibre laser. The powders were contained in their respective hoppers during deposition. A process gas, Argon, was used as both a carrier and shielding gas at 2 l/min and 12 l/min, respectively. The powders were fed through a co-axial brass nozzle head, which was attached to a Kuka robot arm, into the laser melt-pool that was generated by scanning a laser beam of about 2 mm in diameter across the surface on the base plates. This 2 mm laser spot beam had been hanging over the base plate at the stand-off distance of 8 mm while being scanned at 0.3 m/min across. The laser power that was used for cladding GKSS-Mn powders was set at 1000 W. The process set-up is shown in Fig. 2.

During deposition GKSS and Mn powders were in situ alloyed inside the melt-pool. This melt-pool served as a meltingpot. Upon cooling the molten GKSS-Mn would results in a layer that can be characterised of GKSS and Mn. The powder feeder speeds were kept constant at 2 rpm while Mn powder feeder speeds were varied by changing the revolution per min from 0.2 to 1.0 rpm. The combined mass flowrates (in g/min) with respect to powder feeder speeds (rpm)are reported in Fig. 3.

Fig. 3 shows that mass flowrates of GKSS increased with the additions of Mn rpm. These powders were laser processed and the generated clads, similar to the one shown in Fig. 4. These clads were produced on Ti64 substrates. The produced clads were cubes with the dimensions of10x10x7mm as shown in Fig. 4.

Post manufacturing the clads were cut for metallographic preparations and optical observations in the as-built and heat treated state. The samples were labelled 0.00Mn (for GKSS without Mn powder), 0.2Mn, 0.4Mn, 0.6Mn, 0.6Mn, 0.8Mn, and 1.0Mn, respectively for samples that contained Mn. These samples were sectioned into halves, where one half of each sample was studied in the as fabricated state while the remaining half was heat treated, furnace cooled and characterised. Heat treatment was conducted at 1200 °C in an ULTRA-FURN furnace with a holding time of two hours.The produced and heat-treated samples were characterised after being polished to a mirror finish following the recommend laboratory steps of polishing titanium alloy samples. The samples were etched with Kroll's reagent and characterised using the Joel, JSM-6010Plus/LAM scanning electron microscopy (SEM) that was equipped with energy dispersive X-ray analysis (EDS) for appearance and chemical analyses. High magnification SEM images were recorded.

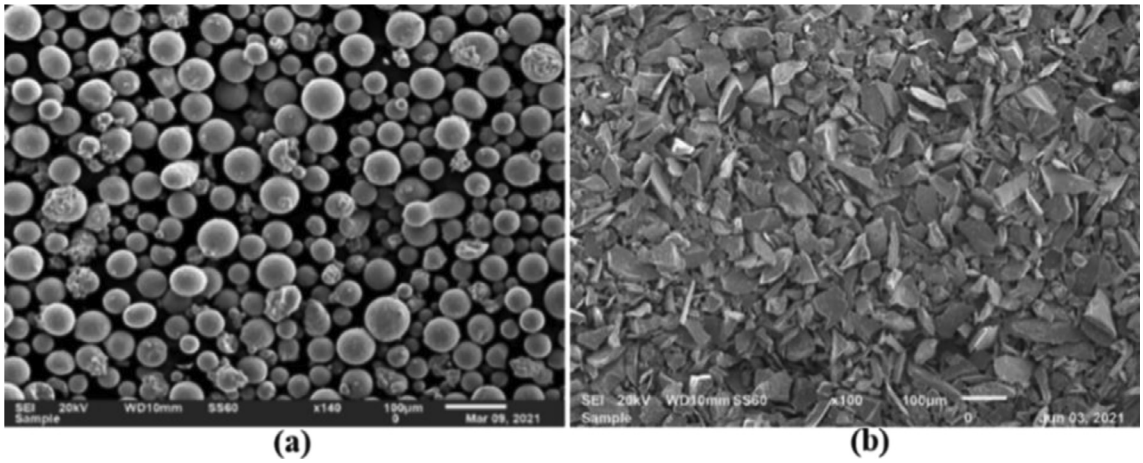

Fig. 1. Feedstock (a) Spherical GKSS castable and (b) Irregular Mn powders.

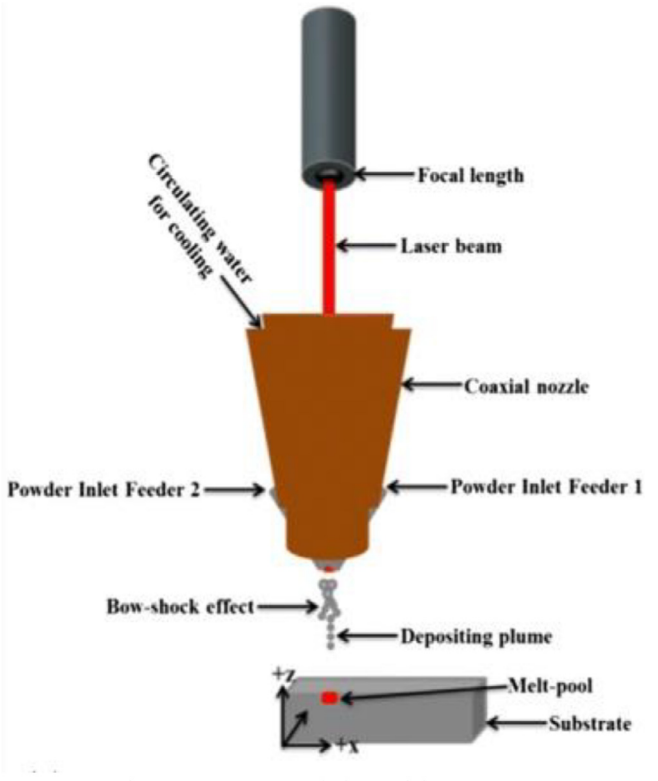

Fig. 2. Laser metal deposition set-up.

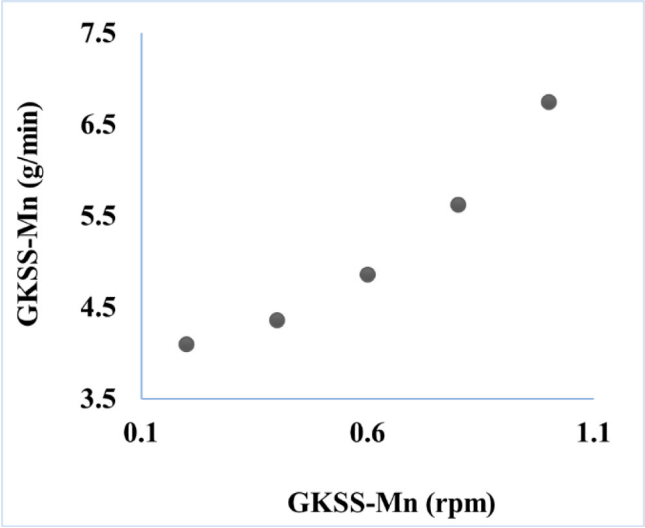

Fig. 3. GKSS-Mn powders before deposition.

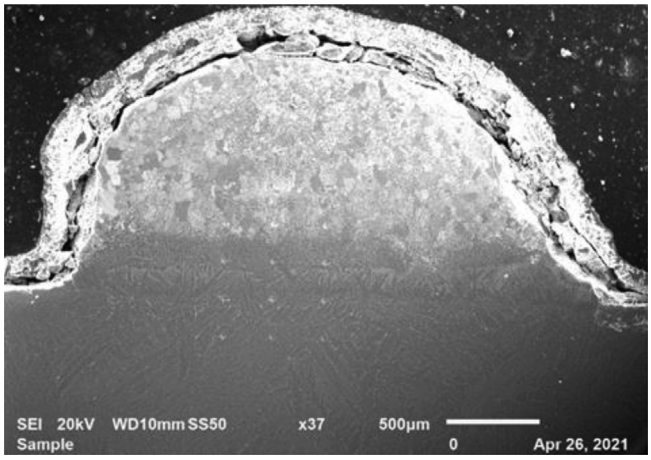

Fig. 4. Single layer clad of GKSS-Mn.

Both Micro-and Nano-hardness measurements were conducted on the samples. The nano-indentation results were necessary as they would indicate which impact Mn would have, if any, on the bulk mechanical properties of the GKSS alloy that was used as a master alloy. The nano-indentation tests were carried out using Anton-Paar TTX-NHT3 nano-indentation tester that has a Berkovich indenting tip with a radius of 20 nm. Before performing tests on all the samples, the machine was calibrated using a fused silica, as a reference sample, following procedure similar to the one distributed by Oliver and Pharr [8]. During indentation, a matrix array of 4 by 4 (totalling 16 indents) were recorded. The loading force was set at 200 mN and was allowed to hold for 20 s before unloading for 20 s.

To determine material properties such as stiffness, indentation hardness and Young's modulus, Pharr [9] method was adopted during the analyses of the displacement curves. Afterwards, the

expressions in equations (1) and (2) were used to calculate the stress and strain, respectively. Other mechanical properties such as ultimate tensile strength (UTS), yield strength (YS) and ductility were subsequently obtained from the stress–strain curves. For micro-hardness, Zwick/Roell (ZHVμ) Vickers' hardness machine with a pin loading of 0.5kgf and dwelling time of 10 s while the produced indents were spaced at 400 μm was used. Three set of indentation (16 in total) were taken across the sample and the average HV value was reported to represent the micro-hardness value of each sample studied.

$$\sigma = \left(\frac{4E_r}{3\pi}\right)\frac{a}{R} \tag{1}$$

$$\varepsilon = \frac{0.2 * a}{R} \tag{2}$$

where, "a" is the indentation radius, "R" is the indenter radius, "Er" is reduced (or effective) modulus, "σ" is the yield stress and "ε" is the strain.

3. Results

3.1. Microstructure

Microstructures were observed using an optical light microscope and images of the microstructures produced were obtained through scanning electron microscopy (SEM) at a magnification of 10 μm. Microstructures of as-built samples are displayed in Fig. 5..

Fig. 5 shows distinct differences in the microstructure of the samples with the increase with Mn content. The microstructure of the GKSS alloy was a typically duplex microstructure (a) and contained segregates of aluminium which were identified as bright white islands. This microstructure can also be characterised of having micro-surface porosity. This surface porosity was also observed for the samples that contained Mn and the dissolution of Mn into the matrix decreased with the increase in Mn. All these samples had homogenous microstructures with grain refinement reported for the sample that contained 2.70 g/min of Mn (c). This microstructural evolution can be summarised as (a)duplex, (b) nearly lamellar, (c) primary dendrites (d) almost Widmanstätten-lamellar (e) Widmanstätten with rods and, finally (f) needle-like Widmanstätten microstructure. The reported microstructures looked homogenous, but the presence of aluminium segregates required further treatment so to dissolve it into the matrix. The samples were heat treated at 1200 °C to produce the desirable and homogenous microstructures. The microstructures of the sample post heat treatment are reported in Fig. 6.

The microstructure of GKSS alloy without the addition of Mn (a) is still duplex and that of 0.2Mn (b) is nearly lamellar with visible lamellar boundaries that appeared to form into for a α_2 + γ lamellae grained microstructure. The formed α_2/γ grains were about 20–40 μm. When Mn was increased to 0.4 rpm (0.4Mn), a lamellae grain microstructure, with fully developed grains of α_2 and γ, was formed (c). It seems that Mn precipitated and formed along the boundaries of the observed α_2/ γ grains forming a black ring around the formed grains (c). These α_2 and γ grains were refined and became smaller with the increasing in Mn (d). The sizes of the α_2/ γ grains reduced by almost half (from 40 to 20 μm) when Mn was increased from 0.4 to 0.6 rpm. The α_2 lamellae grains, which are white in colour and known to be lean in Al, can be contrasted from the γ lamellae grains which are black and reach in Al content. With further increase in Mn, the formed grain boundaries started to dissolve (e) leading to a lamellar-Widmanstätten microstructure. Once dissolved, a fully transformed Widmanstätten microstructure was observed. This was when Mn was increased to 1.0 rpm. The observed Widmanstätten-lamellar microstructure contained α_2/ γ laths (e) which were reduced in size when Mn was increased to 1.0 rpm (f). The formation of the grain boundaries and dissolution of the α_2/ γ laths can only indicate that the microstructure in (f) contained β-precipitates on α_2 + γ grain boundaries. Given the observations in grain formation, refinement, dissolution and precipitation, it is expected that these samples will have different hardness values (following on the Hall-Patch analogy) and tensile properties. The results of the samples' micro-and-nano-indentation are reported next in the mechanical properties section. Microstructures of these findings are summarized in Table 1.

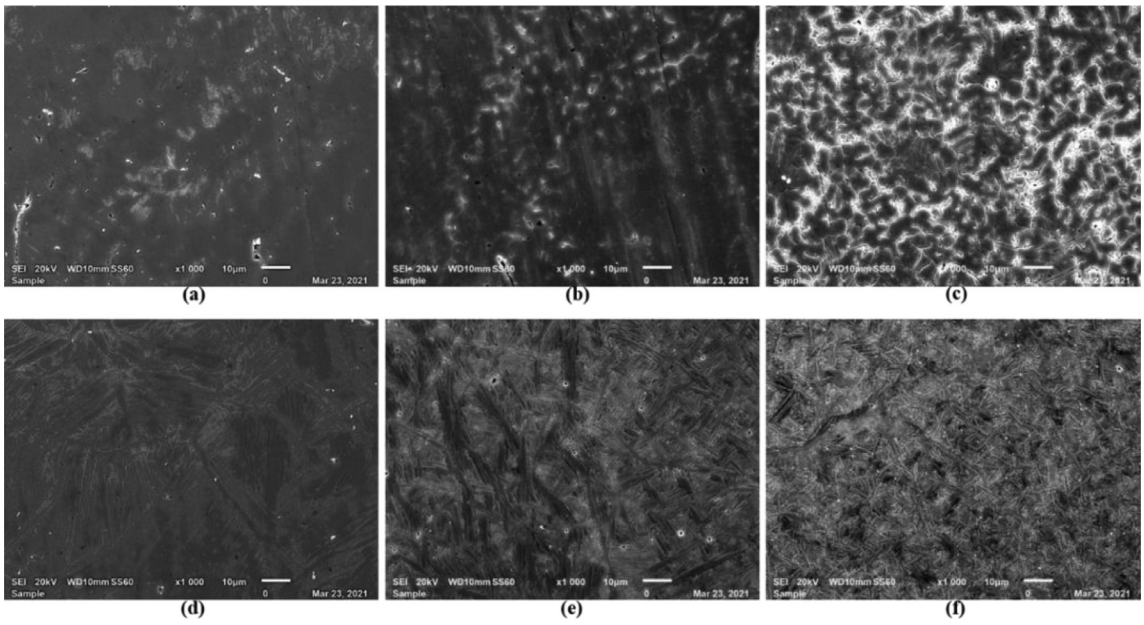

Fig. 5. Laser deposited GKSS-Mn microstructures. (a) 0.0Mn (b) 0.2Mn, (c) 0.4Mn, (d) 0.6Mn, (e) 0.8Mn and (f) 1.0Mn.

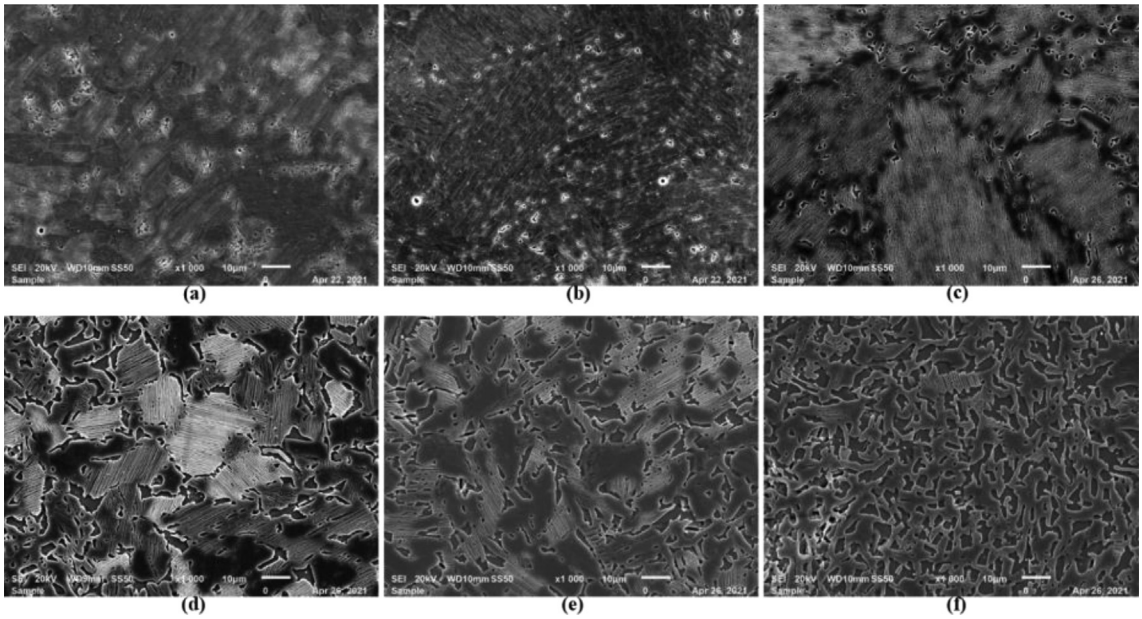

Fig. 6. High resolution microstructures post heat treatment and furnace cooling:(a) 0.0Mn (b) 0.2Mn, (c) 0.4Mn, (d) 0.6Mn, (e) 0.8Mn and (f) 1.0Mn.

Table 1
Microstructures of as built and heat treated alloys.

Figure No.	As-built microstructure	Figure No.	Heat treated
5a	duplex	6a	Duplex
5b	nearly lamellar	6b	nearly lamellar
5c	primary dendrites	6c	Nearly lamellar grains
5d	almost Widmanstätten-lamellar	6d	Equiaxed α_2 + γ grains
5e	Widmanstätten with rods	6e	Widmanstätten with α_2/γ laths
5f	needle-like Widmanstätten microstructure	6f	Widmanstätten with β precipitates

3.2. Mechanical properties

3.2.1. Micro-hardness

The micro-hardness values of both the As-built and heat-treated samples are reported in Fig. 7, and summarised in Table 2. In Fig. 7, it can be observed that microhardness is lower in the heat treated samples while in the As-built, the microhardness increased slightly. This behaviour could be a result of vanadium contamination of the build by the substrate, usually also leading to brittle behaviour.

Fig. 7 presents the hardness profile of the As-built (a) and heat-treated samples (b). All sample show a rather smooth alloy, indicated by both hardness profiles, except for the samples that con-

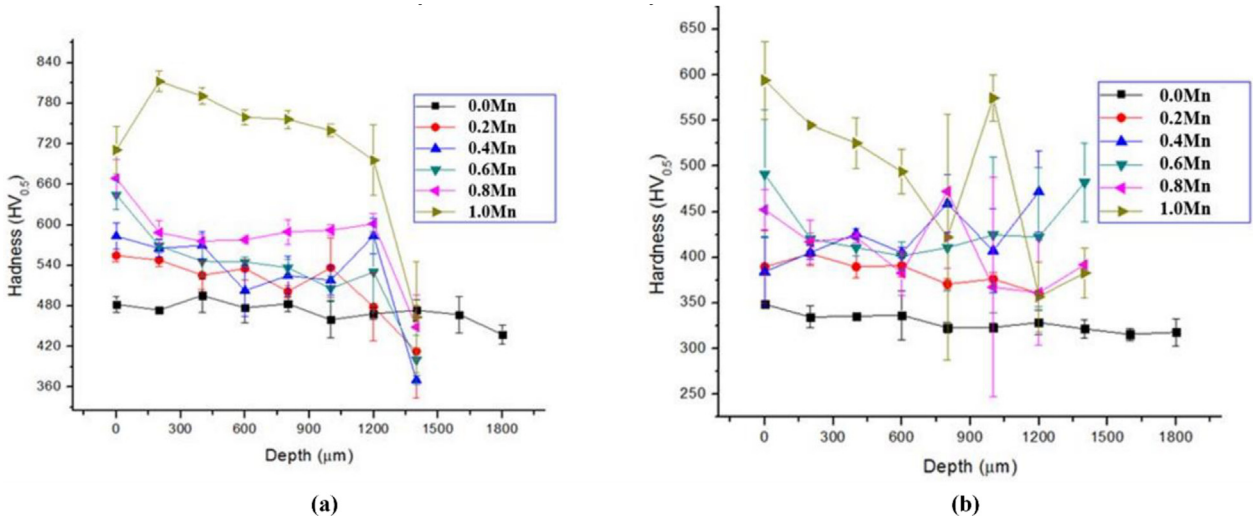

Fig. 7. Micro-hardness plotsAs-built (a) and Heat-treated at 1200 °C (b).

Table 2
Average hardness values.

Sample ID	0.0Mn	0.2Mn	0.4Mn	0.6Mn	0.8Mn	1.0Mn
As-built hardness (HV)	472 ± 16	512 ± 29	527 ± 22	535 ± 23	580 ± 18	716 ± 29
Heat treated (HV)	328 ± 10	383 ± 13	422 ± 25	432 ± 44	407 ± 48	486 ± 40
Mn Content (at. %)	0.00	2.69	5.91	8.07	10.16	12.61

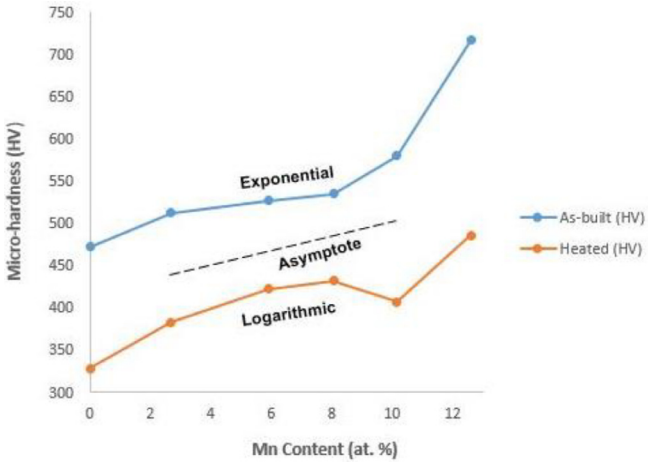

Fig. 8. Average hardness profiles as a function of Mn content.

tained 0.2Mn and 0.4Mn in the As-built state.Their profiles together with samples 0.4Mn and 0.8Mn, in the heat treated state, are wavy. The overall hardness of the samples is reported in Table 1 and summarised in Fig. 8.

Table 2, read in conjunction with Fig. 8, indicate definitely that the hardness of the GKSS alloy for the As-built sample increased exponential with an increase in Mn, and drastically for the 1.0Mn sample. Heat treatment reduced the hardness of all the samples. It can be deducted from Fig. 8 that hardness dropped from exponential increase to logarithmic increase until at a point when hardness dropped from 0.8Mn and significantly increased again for the 1.0Mn sample.

3.2.2. Nano-indentation

The nano-indentation results obtained were analysed and summarised in Table 3.

Table 3 reports mechanical properties of the samples after heat treatment at 1200 °C and furnace cooling. The properties of the alloy in the as cast state are summarised as 410 MPa (YS), 525 MPa (UTS) and 2% elongation [5]. Looking at Table 2, it is deducible that laser processing decreased both the strength and tensile of this alloy. Adding Mn to this alloy and laser processing it led to interesting observations in that already by looking at Table 2, it can be concluded that 0.2Mn (or 2.44 g/min of Mn) is the lower limit while 1.0Mn (or 5.08 g/min of Mn) was the upper limit for increasing %ductility. Both 0.2Mn and 1.0Mn samples have limited ductility (low), but good tensile and yield strengths. In case of 0.4Mn (5.91 g/min Mn) and 0.6Mn (8.07 g/min Mn) the produced alloys have moderate to high ductility but compromised tensile and yield strengths. Most importantly, it appears by adding 10.16 g/min of Mn (0.8Mn), the laser built sample has similar UTS and YS to the 0.00Mn sample, but both have reduced UTS and YS when compared to the as cast sample. Stiffness of other samples differ greatly from that of the 0.00Mn except for 0.8Mn and 0.6Mn samples. These samples are very stiff followed by samples 0.2Mn and 0.4Mn (stiff) and sample 0.2Mn which is stiffer. Modulus of elasticity (Er) show no significant derivable trend for the alloys with Mn, but it can be said that the bulk value show that the samples fall within the same family of material. There is a relationship between stiffness (S) and UTS for sample that have high % ductility. In general Table 2 suggest that there are alloys that will be suitable for application that require material with high yield and tensile strength and ductility (0.0Mn and 0.8Mn) like lightweight values, and those that can be finished into rods would include samples 0.2Mn and 1.0Mn and those UTS decrease with Mn (0.2–0.6) while the 0.4Mn and 0.6Mn alloys would be suitable for valve springs [5].

4. Discussions

In Mn free build, γ duplex uniform microstructure forms post α solidification and solid-state phase transformation reaction $L \rightarrow L + \alpha \rightarrow \alpha \rightarrow \gamma$, which are favourable at Al compositions higher than > 45 %Al and slow cooling rates [10-13]. Microstructure solidifies as α dendrites and transforms to uniform γ duplex structurer. When Mn is added by increasing feed rates from 0.0 to 0.2 rpm, γ rich nearly lamellar microstructure is produced. These microstructures are produced post β phase solidification and solid state phase transformation reaction $L \rightarrow L + \beta \rightarrow \beta \rightarrow \beta + \alpha \rightarrow \alpha \rightarrow \alpha + \gamma$, which takes place at Al compositions below < 45 %Al and slow cooling rates [10–12]. The dendritic equiaxed grain with a lamellar morphology are produced during β solidification at lower Al compositions and slow cooling rates. The Ti rich dendrite cores comprise of β phase while the Al rich interdendritic regions indicate the peritectic precipitations of α phase ($\beta \rightarrow \beta + \alpha$) [10–12]. When Mn feed rate is increased to 0.6 rpm, α rich nearly lamellar microstructures are produced. This nearly lamella microstructure indicates the precipitation of γ within α phase [12,14]. The microstructure also appears similar to basket weave structure in conventional Ti alloys. This microstructure also forms post β solidification and α grain boundary precipitation [11,12]. The Widmanstätten microstructure observed when Mn feed rate is increased to 0.8 rpm indicate the precipitation of α plates from equiaxed β grain boundaries. This leads to structures where β phase comprises the parent grain and α the domain structure

Table 3
Tensile properties of the Heat treated samples.

Sample ID	Er (GPa)	S (mN/nm)	UTS (MPa)	YS (MPa)	% ductility
0.0Mn	169.45	0.93	433	350	4.7
0.2Mn	137.77	0.84	450	400	3.3
0.4Mn	162.4	0.78	375	327	4.6
0.6Mn	128.61	0.90	250	173	4.9
0.8Mn	147.44	0.92	433	393	5.5
1.0Mn	129.69	0.71	437	403	3.7

[15]. When Mn feed rate is finally increased to 1.0 rpm, the grain refinement of the Widmanstätten grains occurs due to the substitution of Mn atoms in Al sublattice sites in BCC Ti-β phase which leads to lattice shrinkage resulting in reduction of grain sizes [16]. Since the solubility of Mn in hexagonal α phase is limited [17], the segregation of Al to α phase Widmanstätten plates becomes favourable while the segregation of Mn to β phase becomes favourable since Mn is also a β phase stabiliser [18].

When heat treatment was carried out at 1200 °C, Mn free duplex structures remained unaffected, with the exception of increased sizes of the Al islands which can be accredited to segregation. Heat treating samples produced using Mn feed rates set at 0.2 rpm further developed the γ rich nearly lamellar structure where it appeared closer to a fully lamellar structure with large lamellae. Heat treating samples produced using Mn feed rates of 0.4 and 0.6 rpm leads to the production of fully lamellar α_2 + γ microstructures. However, the lamellar grains produced at 0.6 rpm are larger than those produced at 0.4. This indicates that heat treatment leads to the reordering of phases through phase transformation reaction $\alpha + \gamma \rightarrow \alpha_2 + \gamma$, which takes place at 1120 °C [17] and produces fully lamellar microstructures[14]. Grain refinement due to increased Mn is accredited by the substitution of Mn into Al sublattices resulting in lattice shrinkage due to the differences between the radius of Mn and Al [16,19]. Heat treatment of Widmanstätten microstructures produced at 0.8 and 1.0 Mn rpm, leads to the refinement of α plates to platelets/laths which have a need-like appearance and are situated on β matrix and grain boundaries. However at Mn feed rate of 1.0 rpm, the Widmanstätten grains are finer, which is accredited to lattice shrinkage due to increased Mn [16]. The transformation with the addition of Mn is supported by the observed UTS and YS values. Significant enough is the fact that, our results conclude a microstructure that has α_2 + γ + β and duplex are necessary for applications that require ductility while lamellar microstructures are in fact brittle. An imbalance between YS and ductility as Mn in the composition increased was observed, with the exception of the heat-treated build produced with Mn feed rate of 0.8 rpm, where maximum calculated ductility was yielded at relatively high UTS and YS. This could be attributed to the good balance in α_2/γ interfaces which promotes ductility through dislocation motion [20] and β which promotes strength [18]. In summary, it was observation and analysis that the produced microstructures are congruent to the resulting Al content with the increase in Mn. Mn feed rates shifted Al towards the left hand side of the TiAl binary phase diagram [10] which is displayed in Fig. 9. This occurred due to the ability of Mn to stabilise Ti-β which occurs on the left hand side of the binary TiAl phase diagram. The left hand has also generally has low Al in the compositions. This is accredited by the increased preferential substitution of Mn on Al sublattices due to Femi levels [9]. The understanding of Ti-Al alloys is that alloys containing 45 Al (at. %) are moderately ductile when compared to (45–48 at. % Al) which are in the preferred range for engineering applications since they have desired ductility and accepted mechanical performance properties while pure gamma alloys are poor ((50 Al (at.%)) in all aspects. The Mn leading to refined microstructures led to increase stiffness and strength leading to a conclusion that the samples can have applications in structural engineering, but they might be brittle. The brittleness or ductile property will be investigated in the future.

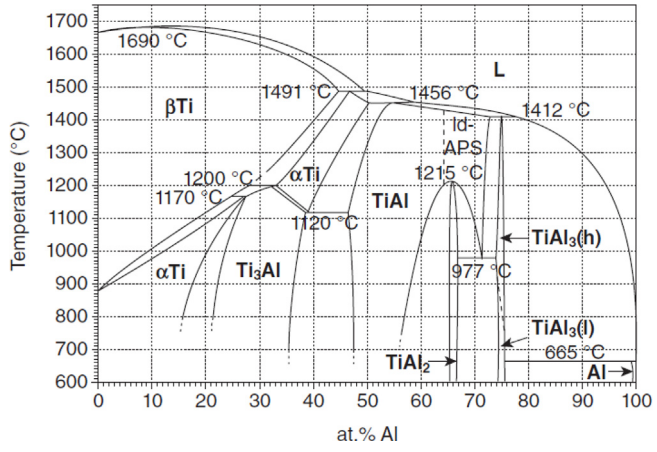

Fig. 9. Binary Ti-Al phase diagram [10].

5. Conclusions

This paper reported on the effects of Mn addition on the mechanical performance properties and microstructure of the castable γ-Ti46.8Al1Cr0.2Si. Previous studies have reported that Mn addition promotes ductility in Ti-Al alloys [16,19], hence it was selected for this study. It is concluded that Mn addition leads to a reduction of Al content and stabilizes the β phase which shifts the microstructural evolution to the left hand side of the Ti-Al binary phase diagram leading to microstructure comprised of γ + α_2 + β. The microstructural evolution is accompanied by increasing microhardness and yield strength. This gives the alloys studied potential for supplication in the automotive industry.

Declaration of Competing Interest

The authors declare that they have no known competing financial interests or personal relationships that could have appeared to influence the work reported in this paper.

Acknowledgements

The authors wish to acknowledge the Council for Scientific and Industrial Research for resources to carry-out this research, the National Research Foundation for funding and Manganese Metal Company (Pty) Ltd., South Africa for their generosity in supplying us with Manganese. Mr Stephen Machete is acknowledged for sharing his intelligence on alloy making, material property testing, and performance as required for structural engineering applications.

References

[1] D. Herzog, V. Seyda, E. Wycisk, C. Emmelmann, Additive manufacturing of metals, Acta Mater. 117 (2016) 371–392.
[2] T. DebRoy, H.L. Wei, J.S. Zuback, T. Mukherjee, J.W. Elmer, J.O. Milewski, A.M. Beese, A. Wilson-Heid, A. De, W. Zhang, Additive manufacturing of metallic components- Process, structure and properties, Prog. Mater Sci. 92 (2018) 112–224.
[3] M. Tlotleng, Microstructural properties of heat-treated LENS in situ additively manufactured titanium aluminide, J. Mater. Eng. Perform. 28 (2) (2019) 701–708.
[4] M. Tlotleng, S.L. Pityana, Effects of Al and heat treatment on the microstructure and hardness of Ti-Al synthesized via in situ melting using LENS, Metals 9 (6) (2019) 1–13.
[5] B.S. Skhosane, M. Tlotleng, S.L. Pityana, Effects of niobium (Nb) on mechanical properties of laser coated Nitinol (NiTi) used for surface modification of Ti6Al4V alloy, MRS Adv. 5 (2020) 1235–1244.
[6] A.N.D. Gasper, C.-S. Smith, A.T. Clare, In-situ synthesis of titanium aluminides by direct metal deposition, J. Mater. Sci. Technol. 239 (2017) 230–239.
[7] O. Schauerte, Titanium in automotive production, Adv. Eng. Mater. 5 (5) (2003) 411–418.
[8] W.C. Oliver, G.M. Pharr, An improved technique for determining hardness and elastic modulus using load and displacement sensing indentation experiments, J. Mater. Res. 7 (1992) 1564–1583.
[9] G.M. Pharr, Measurement of mechanical properties by ultra-low load indentation, Mater. Sci. Eng., A 253 (1-2) (1998) 151–159.

[10] J.C. Schuster, M. Palm, Reassessment of the binary aluminum-titanium phase diagram, Journal of phase equilibria and diffusion 27 (3) (2006) 255–277.
[11] C. McCullough, J. Valencia, C. Levi, R. Mehrabian, Phase equilibria and solidification in Ti-Al alloys, Acta Metall. 37 (5) (1989) 1321–1336.
[12] V. Küstner et al., 'Gamma titanium aluminides 2003', 2003.
[13] F. Appel, R. Wagner, Microstructure and deformation of two-phase γ-titanium aluminides, Materials science and engineering: r: reports 22 (5) (1998) 187–268.
[14] F. Appel, J.D.H. Paul, M. Oehring, Gamma titanium aluminide alloys. Wiley Online, Library (2011).
[15] T. Cheng, M. Loretto, The decomposition of the beta phase in Ti–44Al–8Nb and Ti–44Al–4Nb–4Zr–0.2 Si alloys, Acta Mater. 46 (13) (1998) 4801–4819.
[16] S. Shu, F. Qiu, B. Xing, S. Jin, Y. Wang, Q. Jiang, Study of effect of Mn addition on the mechanical properties of Ti2AlC/TiAl composites through first principles study and experimental investigation, Intermetallics 28 (2012) 65–70.
[17] J.L. Murray, The Mn− Ti (Manganese-Titanium) system, Bulletin of Alloy Phase Diagrams 2 (3) (1981) 334–343.
[18] F. Holden, H. Ogden, R. Jaffee, Heat treatment, structure, and mechanical properties of Ti-Mn alloys, JOM 6 (2) (1954) 169–184.
[19] Q. Wang, H. Ding, H. Zhang, R. Chen, J. Guo, H. Fu, Influence of Mn addition on the microstructure and mechanical properties of a directionally solidified γ-TiAl alloy, Mater. Charact. 137 (2018) 133–141.
[20] S.-W. Kim, Y.-S. Na, J.-T. Yeom, S.E. Kim, Y.S. Choi, An in-situ transmission electron microscopy study on room temperature ductility of TiAl alloys with fully lamellar microstructure, Mater. Sci. Eng., A 589 (2014) 140–145.